

This is an Open Access document downloaded from ORCA, Cardiff University's institutional repository: <https://orca.cardiff.ac.uk/id/eprint/109805/>

This is the author's version of a work that was submitted to / accepted for publication.

Citation for final published version:

Sun, Qiliang, Alves, Tiago , Lu, Xiangyang, Chen, Chuanxu and Xie, Xinong 2018. True volumes of slope failure estimated from a Quaternary mass-transport deposit in the northern South China Sea. *Geophysical Research Letters* 45 (6) , pp. 2642-2651. 10.1002/2017GL076484

Publishers page: <http://dx.doi.org/10.1002/2017GL076484>

Please note:

Changes made as a result of publishing processes such as copy-editing, formatting and page numbers may not be reflected in this version. For the definitive version of this publication, please refer to the published source. You are advised to consult the publisher's version if you wish to cite this paper.

This version is being made available in accordance with publisher policies. See <http://orca.cf.ac.uk/policies.html> for usage policies. Copyright and moral rights for publications made available in ORCA are retained by the copyright holders.



# True volumes of slope failure estimated from a Quaternary mass-transport deposit in the northern South China Sea

Qiliang Sun<sup>a,b,c</sup>, Tiago Alves<sup>d</sup>, Xiangyang Lu<sup>a,c</sup>, Chuanxu Chen<sup>e</sup>, Xinong Xie<sup>a,c</sup>,

<sup>a</sup>*College of Marine Science and Technology, China University of Geosciences (CUG), Wuhan, Hubei 430074, PR China;*

<sup>b</sup>*Laboratory for Marine Mineral Resources, Qingdao National Laboratory for Marine Science and Technology, Qingdao 266061, China;*

<sup>c</sup>*Key Laboratory of Tectonics and Petroleum Resources, China University of Geosciences, Ministry of Education, Wuhan 430074, China;*

<sup>d</sup>*3D Seismic Lab, School of Earth and Ocean Sciences, Cardiff University, Main Building, Park Place, Cardiff CF10 3AT, United Kingdom;*

<sup>e</sup>*Sanya Institute of Deep-sea Science and Engineering, Chinese Academy of Sciences, Sanya 572000, China;*

## Highlights:

1. Volume of turbidites generated by slope failure and volume of shear compaction during landslide emplacement are estimated for the first time;
2. The original volume of failed slope sediment is ~18% larger than the volume estimated by only using seismic reflection data;
3. Failed sediments are more consolidated than 'background' slope sediment at shallow burial depths.

This article has been accepted for publication and undergone full peer review but has not been through the copyediting, typesetting, pagination and proofreading process which may lead to differences between this version and the Version of Record. Please cite this article as doi: 10.1002/2017GL076484

## **Abstract**

Submarine slope failure can mobilize large amounts of seafloor sediment, as shown in varied offshore locations around the world. Submarine landslide volumes are usually estimated by mapping their tops and bases on seismic data. However, two essential components of the total volume of failed sediments are overlooked in most estimates: a) the volume of sub-seismic turbidites generated during slope failure and b) the volume of shear compaction occurring during the emplacement of failed sediment. In this study, the true volume of a large submarine landslide in the northern South China Sea is estimated using seismic, multibeam bathymetry and ODP/IODP well data. The submarine landslide was evacuated on the continental slope and deposited in an ocean basin connected to the slope through a narrow moat. This particular character of the sea floor provides an opportunity to estimate the amount of strata remobilized by slope instability. The imaged volume of the studied landslide is  $\sim 1035 \pm 64 \text{ km}^3$ ,  $\sim 406 \pm 28 \text{ km}^3$  on the slope and  $\sim 629 \pm 36 \text{ km}^3$  in the ocean basin. The volume of sub-seismic turbidites is  $\sim 86 \text{ km}^3$  (median value) and the volume of shear compaction is  $\sim 100 \text{ km}^3$ , which are  $\sim 8.6\%$  and  $\sim 9.7\%$  of the landslide volume imaged on seismic data, respectively. This study highlights that the original volume of the failed sediments is significantly larger than that estimated using seismic and bathymetric data. Volume loss related to the generation of landslide-related turbidites and shear compaction must be considered when estimating the total volume of failed strata in the submarine realm.

## **Keywords:**

South China Sea, Submarine slope failure, Mass-transport deposits, Volume balance, Shear compaction

## **Plain Language Summary**

Submarine slope failure can mobilize large amounts of seafloor sediments. Submarine landslide volumes are usually estimated by mapping their tops and bases on seismic data. However, two essential components of the total volume of failed sediments are overlooked in most estimates: a) the volume of sub-seismic turbidites generated during slope failure and b) the volume of shear compaction occurring during the emplacement of failed sediment. In this study, the true volume of a large submarine landslide in the northern South China Sea is estimated using seismic, multibeam bathymetry and ODP/IODP well data. The volume of sub-seismic turbidites and the volume of shear compaction in the northern South China Sea are  $\sim 8.6\%$  and  $\sim 9.7\%$  of the landslide volume imaged on seismic data, respectively. This

study is important by showing that the original volume of the failed sediments is significantly larger than that estimated using seismic and bathymetric data. Volume loss related to the generation of landslide-related turbidites and shear compaction must be considered when estimating the total volume of failed strata in the submarine realm.

## Introduction

Submarine landslides typically record complex deformation and downslope transport processes, with slides, slumps, debris flows and turbidity currents being often documented on the world's continental margins (e.g. Dott, 1963; Nardin et al., 1979). The three latter processes are considered in the literature as generating the main components of mass-transport deposits (MTDs), and can be identified on seismic data (e.g. Nardin et al., 1979; Moscardelli and Wood, 2008; Bull et al., 2009). In addition, turbidites generated during slope failure are commonly observed on sediment cores as they cover very large areas of continental slopes and ocean basins (e.g. Piper et al., 1997; Masson et al., 2002; Owen et al., 2007). Detailed estimates of the volume of MTDs ( $V_m$ , see Text S1 for the detailed terminology definition; Fig. 1a) on seismic data, and morphological analyses of seafloor scars using multibeam bathymetric data, are key to calculate the residual volume of failed strata after their emplacement ( $V_r$ , Fig. 1) (e.g. ten Brink et al., 2006; Lamarche et al., 2008; Alves and Cartwright, 2009; Völker, 2010; Calvès et al., 2015). However, residual failed volumes are probably larger than the primary volume of failed strata ( $V_m$ , Fig. 1a), because landslide-related turbidites can seldom be imaged in detail on seismic data. The sub-seismic nature of these turbidites, and the limited coverage of boreholes on many a continental margin, make the estimate of the volume of turbidites ( $V_t$ ) derived from discrete instability events virtually impossible.

The volume of MTDs ( $V_m$ ) interpreted on seismic and bathymetric data is usually considered in the literature as the original volume of totally failed sediments ( $V_o$ ). Nevertheless, the parameter  $V_o$  usually comprises all remobilized sediment, i.e. the initial volume of failed strata and the sediment incorporated in the landslide during its downslope transport. Conversely, volume loss ( $V_l$ ) caused by shear compaction should also be taken into account (but rarely is) when characterizing MTD emplacement (Figs. 1b-c). Around 20% of water and associated porosity are lost in MTDs when comparing these with undeformed strata (Shipp et al., 2004). Hence, when only seismic data are available, calculations of the original (failed) volume of MTDs are likely to return much smaller values than the true volume of remobilized sediments, as the volumes of turbidite ( $V_t$ ) and shear compaction ( $V_l$ ) are neglected on most seismic-data

interpretations. This caveat has an impact on geo-hazard assessments on continental slopes, especially when estimating tsunami magnitude, a parameter greatly linked to the initial volume of failed sediment (e.g. Locat et al., 2004; Text S1). Furthermore, to accurately calculate the original volume of failed seafloor strata is important when modeling landslide-generated turbidites, many of which can disrupt cables and other infrastructure placed on the sea floor (Pope et al., 2017).

In this study the evacuated zone of an MTD generated on the continental slope of the northern South China Sea, and its depositional zone in an ocean basin, are imaged using a large seismic dataset (Fig. 2a). These two areas (slope and ocean basin) are separated by a structural high (continent-ocean boundary: COB), being only connected through a narrow bottle-neck pathway, or moat (Fig. 2a). Such a configuration provides an opportunity to estimate the volume of strata accumulated as ‘sub-seismic’ turbidities. In addition, volume loss by shear compaction was calculated using previously acquired ODP/IODP well data. This study is the first to address ‘sub-seismic’ turbidite volumes and the total volume of sediment lost during the emplacement of MTDs. Our results are of key significance to other slope failures on the world’s continental margins.

## Data and methods

A total of 35,200 km of 2-D and 6750 km<sup>2</sup> of 3-D post-stack seismic data are utilized in this study (Fig. 2a). The 2-D seismic data were acquired from 1987 to 2002 with main frequencies of ~30 Hz in the ocean basin, ~35 Hz and ~45 Hz on the continental slope. Vertical resolutions are ~13 m, ~11 m and ~9 m, respectively. The 3-D seismic data has a main frequency of ~45 Hz and thus a vertical resolution of ~9 m. In this paper, a primary-wave velocity ( $V_p$ ) of ~1540 m/s, derived from ODP site 1146 which is located in the study area (see Fig. 2a for location), is used in our time-depth conversions. In parallel, ~37,500 km<sup>2</sup> of multibeam bathymetric data, acquired in 2008 by a SeaBeam 2112 multibeam echo-sounder, are used in this work. The depth accuracy of the SeaBeam 2112 data is better than 0.5% of the water depth in the study area, and the raster grid was sampled with a ~100 m resolution (cell size).

ODP/IODP data from the Amazon Fan (Site 941A of ODP 155) and Gulf of Mexico (U 1322B, U1323A and U1324B of IODP 308), from similar depositional environments to the northern South China Sea (located in the deep-water areas and dominated by fine-grained sediments, Table S1), are used as analogues to the study area. IODP Site U1432, located on a debris fan, is not used in this study because it was not cored or logged (Fig. 2a). Sediment porosity in the interpreted ODP/IODP wells was calculated

from the equation  $\phi = (\rho_b - \rho_g) / (\rho_w - \rho_g)$ , where  $\rho_g$  and  $\rho_w$  are respectively the pore fluid density (1.03 g/cm<sup>3</sup>) and the solid grain density (2.7 g/cm<sup>3</sup>) (Dugan, 2012). The tops and bases of MTDs interpreted on Schlumberger's Geoframe 4.5<sup>®</sup> were exported into the Generic Mapping Tools program (GMT) of Wessel and Smith (1998). MTD volumes were calculated using this latter software (Fig. 3a, Text S2).

Fifty-two (52) profiles with a spacing of 2-5 km, crossing the headwall scarp of the main MTD, were also used to reconstruct seafloor bathymetry prior to slope failure (Text S3; Figs. S1-S2). After reconstructing the slope paleo-bathymetry, the volume of sediment evacuated from the slope was calculated by comparing the present-day seafloor with its reconstructed counterpart (Figs. 3b-c; Text S3).

For the calculation of shear compaction we used best-fit curves of porosities for normally compacted fine-grained sediments ( $P_n(h)$ ), and failed fine-grained sediments ( $P_m(h)$ ), on the ODP/IODP borehole data previously mentioned (See Text S2 for details):

$$P_n(h) = -0.077 \ln(h) + 0.8953 \quad (1)$$

$$P_m(h) = -0.048 \ln(h) + 0.7079 \quad (2)$$

Where  $h$  is the depth in mbsf. Porosity losses ( $P_{ave}(h)$ ) are mainly caused by shear compaction during the emplacement of failed sediment (for a defined burial depth), and are expressed by Equation (3):

$$P_{ave}(h) = P_n(h) - P_m(h) = -0.029 \ln(h) + 0.1874 \quad (3)$$

The average porosity loss ( $\Delta P_{ave}$ ) for a MTD with a thickness  $H_2$  can be calculated using Equation (4):

$$\Delta P_{ave} = \left( \int_1^{H_2} P_{ave}(h) \right) / (H_2 - 1) \quad (4)$$

Where the  $\Delta P_{ave}$  is calculated from a depth of 1 mbsf, and following 1-m steps.

Therefore, the lost thickness ( $\Delta H$ ) for a certain location with an MTD showing a thickness  $H_2$ , can be expressed by:

$$\Delta H = \Delta P_{ave} \times H_2 / (1 - \Delta P_{ave}) \quad (5)$$

By integrating  $\Delta H$  for every unit area ( $ds$ ), the lost volume caused by shear compaction can be calculated using the Generic Mapping Tools program (GMT) of Wessel and Smith (1998).

## Mass-transport deposits and their imaged volume on seismic data

On the northern continental slope of the South China Sea (Fig. 2a) are observed large headwall scarps and associated mass-transport deposits characterized by chaotic seismic reflections (Figs. 2c-d; Figs. S3-S4). Fine-grained sediments (mud) predominate in shallow strata (< 400 mbsf) (Gong et al., 1997; Zhu et al., 2009; Xie et al., 2013; Sun et al., 2017a). The study area comprises two regions, a slope region and the ocean basin, which are connected through a 9 km- to 14 km-wide moat (Fig. 2a).

The continental slope covers an area of  $\sim 5500 \text{ km}^2$  and shows headwall scarps that are 10 m to  $\sim 185 \text{ m}$  tall (Figs. 2a-b). The volume of failed sediment accumulated on the continental slope, as interpreted on seismic data, is  $\sim 406 \pm 28 \text{ km}^3$  (Fig. 3a). Any errors in volume estimates for failed sediment are chiefly caused by the resolution limits of the seismic data. Hence, a value of half the theoretical seismic resolution ( $\sim 5 \text{ m}$  on the continental slope and  $\sim 6.5 \text{ m}$  in the ocean basin) are adopted in this work as minimum error values. Because the scarps of slope failures are fresh in the study area, differences in sedimentation rates within and outside the scarps are likely minor. Therefore, the depleted (or evacuated) MTD volume in this work takes into account the height of headwall scarps on the present-day seafloor, and returns a value of  $\sim 715 \text{ km}^3$  (Figs. 3b-c; Text S3). This means that a large volume of failed sediment was transported into the ocean basin through the moat imaged in Fig. 3a.

The ocean basin is a depositional area. It shows a maximum thickness just outside the moat (Fig. 3a) and scatters from this point to form a debris fan with  $\sim 5600 \text{ km}^2$  (Figs. 2a, 3a). This debris fan gradually wedges out from the moat (Fig. 2d). The estimated MTD volume in the ocean basin is  $\sim 629 \pm 36 \text{ km}^3$  considering a seismic-data resolution of  $\sim 13 \text{ m}$  for this region. Therefore, the total volume of the MTD ( $V_m$ ) imaged on seismic data, including any deposits remobilized in the slope area, is  $\sim 1035 \pm 64 \text{ km}^3$  (i.e.,  $406 \pm 28 \text{ km}^3 + 629 \pm 36 \text{ km}^3$ ). An important observation is that a volume discrepancy is clear between the evacuated zone on the continental slope ( $\sim 715 \text{ km}^3$ ) and the depositional zone in the ocean basin (debris fan:  $\sim 629 \pm 36 \text{ km}^3$ ). This discrepancy ranges from  $\sim 50 \text{ km}^3$  to  $\sim 122 \text{ km}^3$  (Fig. 3a-c).

## Volume lost by shear compaction

Shear compaction during slope failure can cause overconsolidation of emplaced MTDs. This has been confirmed by identifying losses in porosity and water content in failed materials (Piper et al., 1997; Shipp et al., 2004), by core observations (Tripsanas et al., 2008; Strasser et al., 2011), and by observations of trapped free gas underneath failed material (Sun et al., 2017b). Multiple DSDP/ODP/IODP wells have

been drilled through failed sediment (e.g. Piper et al., 1997; Strasser et al., 2011; Dugan, 2012). Amongst them, only a few wells with robust evidence for similar depositional environments to the study area are used in this work (see Table S1).

The porosity of undeformed and failed sediment (MTD) is calculated here using sediment bulk densities and the equations previously mentioned. Significantly, the porosities of undeformed and failed sediment both follow logarithmic curves and reveal relatively high best-fit coefficients ( $R^2$ ) of 0.76 and 0.63, respectively (Fig. 3d). These best-fit curves show that porosity quickly increases from the sea floor to ~9 mbsf, to then gradually decrease below this latter depth (Fig. 3d). Conversely, the porosity difference between the MTD and 'background' slope sediment is less than 1% below ~455 mbsf (Fig. 3d). As a result of our estimates, the volume loss caused by shear compaction during slope failure is calculated as ~100 km<sup>3</sup> in the study area (Fig. 3e; Text S2).

## Discussion

The amount of volume loss caused by shear compaction is chiefly related to the properties of the sediment in the MTDs, namely their lithology. Even small shear stresses will cause significant porosity and volume losses in fine-grained sediment (Piper et al., 1997; Shipp et al., 2004). Therefore, we must emphasize that the best-fit curves used in this study are mainly applied to depositional environments in which fine-grained sediments predominate (Fig. 3d). When calculating volume loss by shear compaction, landslide-related turbidites are not considered, because: (1) they do not experience shear compaction and (2) the best-fit curve calculated in Fig. 3d is derived from analyzing failed material that is already emplaced (slides, slumps and debris). In the study area, the volume reduction caused by shear compaction is ~100 km<sup>3</sup> or ~9.1% to 10.3% (median value of 9.7%) of the total volume of the MTD imaged on seismic data. This value (~100 km<sup>3</sup>) is larger than 74% of the known volume of slope failures, according to the statistical data provided by Moscardelli and Wood (2015). Thus, shear compaction must be considered when calculating the volume of emplaced MTDs, especially when dealing with large slope failures.

Porosity curves of 'background' slope sediment vs. MTDs indicate that shear compaction plays an important role in reducing porosity in shallow (failed) strata (Fig. 3d). As burial depth increases, the porosity difference between 'background' slope and failed sediment becomes small, probably due to changes in the texture of failed sediment during burial (e.g. Ogiesola and Hammes, 2012; Alves et al., 2014). If one considers different depositional environments to the northern South China Sea's, the best-fit

curves will not strictly be the same as in Fig. 3d, but should nonetheless show similar trends to this latter figure. In the study area, the effect of shear compaction is healed with depth and the failed sediment tends to normal compaction at ~640 mbsf (Fig. 3d).

Few published cases show clear boundaries for evacuated and depositional zones of MTDs, a caveat resulting in the impossibility of calculating turbidite volumes using seismic and bathymetric data alone. Normally, the volume of MTDs evacuated from the continental slope is expected to equal the depositional volume in the ocean basin. Because of the sub-seismic resolution of most discrete turbidite flows, they cannot be directly imaged and volume estimates must be gathered from subtracting MTD volumes between evacuated and depositional zones. In this study, the volume difference between the evacuated sediment on the slope and the material deposited in the ocean basin can be used as a first-order estimate for turbidite volume, because the deposits in the ocean basin show very minor evidence for erosion and slope entrainment. Thus, the amount of sediment incorporated in the MTD emplaced in the ocean basin did not contribute significantly to its (imaged) volume on seismic data. Considering calculation errors and the resolution of the seismic data interpreted in this work, a minimum of 50 km<sup>3</sup> and a maximum of 122 km<sup>3</sup> are estimated to be the volume of turbidites scattered in the ocean basin. Therefore, turbidites associated with slope failure are ~4.5% - ~12.6% of the imaged MTD volume (median value of 8.6%) in the study area.

Turbidite rates (the volume of failed sediment transformed in turbidites) are variable on a case-by-case basis. From the limited cases reported in the literature, the Storegga Slide shows turbidite rates ranging from 7.8% to 10.4% (Haflidason et al., 2005), values that are similar to the turbidite rates calculated in this work. However, some major landslides do not show any associated turbidites (e.g. the Sahara Slide on the northwest African continental margin; Georgiopolou et al., 2010). In some steeper continental slopes, turbidite rates may be much larger than those reported here as turbidity currents often incorporate significant volumes of seafloor sediment. The precise factors controlling the volume of failed sediment (debris flow) transferred into turbidite flows are still unknown, with the downslope velocity of the failed sediment, the nature (lithology) of failed sediment, water depth and slope angle being speculated as key parameters in this transfer. Considering that the two previous cases (the Storegga Slide and the study area) have similar turbidite rates, and other slope failures (volume > 1000 km<sup>3</sup>) located in deep-water regions with gentle slope gradients are similar to the northern South China Sea, the turbidite rates calculated in this work can be used as a reference to large slope failures. A large amount of turbidites (e.g. 1890 - 5292 km<sup>3</sup>

for Makran Accretionary Complex) would therefore be expected in these large-scale slope failures (See Table S2 for the possible turbidite contents of large-scale slope failures (imaged volume  $\geq 1000 \text{ km}^3$ ) (Dingle, 1977; Dingle, 1980; Trincardi and Argnani, 1990; Popenoe et al., 1993; Piper et al., 1997; Torelli et al., 1997; Niemi et al., 2000; Wynn et al., 2000; Collot et al., 2001; Haflidason et al., 2004; Lee et al., 2004; Frey Martinez et al., 2005; Gee et al., 2006; Vanneste et al., 2006; Hjelstuen et al., 2007; Burg et al., 2008; Lamarche et al., 2008; Chaytor et al., 2010; Owen et al., 2010; Mosher et al., 2012; Denne et al., 2013; Armandita et al., 2015; Calvès et al., 2015; Leslie and Mann, 2016)). It is worth to note that there are still some uncertainties about the volume estimates for turbidites in the study area. These uncertainties derive from cumulative errors when estimating the volume of sediment originally evacuated from the slope, and unknown differences in the physical properties of evacuated and deposited materials. To obtain a final value for turbidite volume, a large coverage of high-resolution 3D seismic and borehole data are necessary in the future studies.

Apart from the realization that MTDs are an important stratigraphic component of continental margins (they can reach  $\sim 70\%$  of their total volume of sediments; Maslin et al., 2004; Moscardelli and Wood, 2008), this study has significant implications to, at least, four key aspects: (1) when accurately calculating the volumes of MTDs, a piece of information that is important to the modeling of sediment transport and distribution processes in deep-water margins; (2) when modeling tsunami height and distribution, as the initial volume of failed sediment (Text S1), together with water depth, initial sediment acceleration, sediment type and slope gradient, are important parameters influencing the magnitude of landslide-triggered tsunamis (Locat et al., 2004). Most published data, using only imaged volumes ( $V_m$ ) for MTDs, have consistently returned modeled tsunami magnitudes that are lower than their witnessed heights, e.g. 1998 Papua New Guinea tsunami (Synolakis et al., 2002), 1929 Grand Bank (Fine et al., 2005) and 1964 southern Alaska (Brothers et al., 2016). For example, the modeled height for the 1998 Papua New Guinea tsunami was 20% - 50% lower than the values observed in the field (Synolakis et al., 2002), a result of systematic underestimations of the volume of MTDs associated with the tsunami; (3) deep-water cables can be disrupted by landslide-generated turbidity currents (Carter et al., 2012; Pope et al., 2017). The volume of turbidites ( $V_t$ ) is, therefore, a significant parameter when modeling turbidity-current dynamics in deep-water areas; (4) the volume distribution and physical changes of sediments (e.g. decreases of porosity and permeability of MTDs; Shipp et al., 2004; Piper et al., 1997; Sun et al., 2017b) are key to a correct assessment of seal competence in hydrocarbon-rich areas.

## **Conclusions**

Turbidites generated during slope instability events, and shear compaction during landslide emplacement, are estimated for the first time using a comprehensive dataset from the northern South China Sea. They have similar orders of magnitude and are both important components of the original volume of failed sediment. The original volume of failed sediment is ~18% higher than the imaged volume on seismic reflection data. Therefore, landslide-related turbidites and shear compaction cannot be overlooked. Volume estimates of slope failure are themselves, an important component in deep-water sedimentological studies and have serious implications to the modeling of transport processes and dynamics of failed sediments. They also have implications to the modeling of landslide-generated tsunamis.

This study shows that failed sediment is overconsolidated at shallow burial depths, and depositional compaction has a minor influence on failed strata when compared to 'background' slope units. As burial depth increases, the compaction (porosity loss) rates of deformed and undeformed sediments tend to even out. Hence, this study provides a first approach to estimating the original volume of MTDs, and how to calculate sub-seismic turbidite and shear compaction volume losses. Nevertheless, we must stress that other factors influence the volume estimate of failed sediments. Shear compaction of mixed sand-mud and sandstone-rich MTDs, the precise controlling factors generating landslide-related turbidites, errors when calculating evacuated volume, and the influence of shear compaction on volume estimates of turbidites, should be key parameters to assess in future work.

## **Acknowledgements**

This work was supported by the National Scientific Foundation of China (Grant Nos. 91528301 and 41676051), the Programme of Introducing Talents of Discipline to Universities (No. B14031), and Fundamental Research Funds for the Central Universities-the China University of Geosciences (Wuhan) (No. CUG160604). We thank the China National Offshore Oil Company, the Guangzhou Marine Geological Survey and the Second Institute of Oceanography for permission to release the data. The reflection seismic/multibeam bathymetric data may be requested from these company/institutes. The Generic Mapping Tools (GMT) (Wessel and Smith 1998) was used to compile Figure 3. Editor Andrew V. Newman and two anonymous reviewers are thanked for their invaluable comments and suggestions, which greatly improve the manuscript. Finally, Lorena Moscardelli from the Statoil Research and Technology,

Joe Cartwright from the University of Oxford and David J.W. Piper from the Bedford Institute of Oceanography are thanked for their discussions and suggestions on the original version of this paper. ODP/IODP data can be accessed via the database (<http://iodp.tamu.edu/OVERVIEW/>).

## References

- Alves, T. M., and Cartwright, J.A., 2009, Volume balance of a submarine landslide in the Espírito Santo Basin, offshore Brazil: quantifying seafloor erosion, sediment accumulation and depletion: *Earth and Planetary Science Letters*, v. 288, p. 572-580, doi:10.1016/j.epsl.2009.10.020.
- Alves, T.M., Kurtev, K., Moore, G.F., and Strasser, M., 2014, Assessing the internal character, reservoir potential, and seal competence of mass-transport deposits using seismic texture: A geophysical and petrophysical approach: *AAPG Bulletin*, v. 98, p. 793–824, doi:10.1306/09121313117.
- Armandita, C., Morley, C.K., and Rowell, P., 2015, Origin, structural geometry, and development of a giant coherent slide: The South Makassar Strait mass transport complex: *Geosphere*, v. 11, p. 376-403, doi: 10.1130/GES01077.1.
- Brothers, D.S., Haeussler, P.J., Liberty, L., Finlayson, D., Geist, E., Labay, K., and Byerly, M., 2016, A submarine landslide source for the devastating 1964 Chenega tsunami, southern Alaska: *Earth and Planetary Science Letters*, v. 438, p. 112-121, doi: 10.1016/j.epsl.2016.01.008.
- Bull, S., Cartwright, J., and Huuse, M., 2009, A review of kinematic indicators from mass-transport complexes using 3D seismic data: *Marine and Petroleum Geology*, v. 26, p. 1132–1151, doi:10.1016/j.marpetgeo.2008.09.011.
- Burg, J.P., Bernoulli, D., Smit, J., Dolati, A., and Bahroudi, A., 2008, A giant catastrophic mud-and-debris flow in the Miocene Makran: *Terra Nova*, v. 20, p. 188-193, doi:10.1111/j.1365-3121.2008.00804.x.
- Calvès, G., Husse, M., Clift, P.D., and Brusset, S., 2015, Giant fossil mass wasting off the coast of West India: The Nataraja submarine slide: *Earth and Planetary Science Letters*, v. 432, p. 265-272, doi: 10.1016/j.epsl.2015.10.022.
- Carter, L., Milliman, J.D., Talling, P.J., Gavey, R., and Wynn, R.B., 2012, Near-synchronous and delayed initiation of long run-out submarine sediment flows from a record breaking river flood, offshore Taiwan: *Geophysical Research Letters*, v. 39, p. L12603, doi: 10.1029/2012GL051172.
- Chaytor, J.D., Twichell, D.C., Lynett, P., and Geist, E.L., 2010, Distribution and tsunamigenic potential of submarine landslides in the Gulf of Mexico, in Mosher, D.C., Shipp, R.C., Moscardelli, L., Chaytor, J.D., Baxter, C.D.P., Lee, H.J., and Urgeles, R., eds., *Submarine Mass Movements and Their Consequences: Dordrecht, Springer, Advances in Natural and Technological Hazards Research*, v. 28, p. 745-754.
- Collot, J.Y., Lewis, K., and Lamarche, G., 2001, The giant Ruatoria debris avalanche on the northern Hikurangi margin, New

- Zealand: Result of oblique seamount subduction: *Journal of Geophysical Research*, v. 106, p. 19271-19297, doi: 10.1029/2001JB900004.
- Denne, R.A., Scott, E.D., Eickhoff, D.P., Kaiser, J.S., Hill, R.J., and Spaw, J.M., 2013, Massive Cretaceous-Paleogene boundary deposit, deep-water Gulf of Mexico: New evidence for widespread Chicxulub-induced slope failure: *Geology*, v. 41, p. 983-986, doi: 10.1130/G34503.1.
- Dingle, R.V., 1977, The anatomy of a large submarine slump on a sheared continental margin (SE Africa): *Journal of the Geological Society*, v. 134, p. 293-310, doi: 10.1144/gsjgs.134.3.0293.
- Dingle, R.V., 1980, Large allochthonous sediment masses and their role in the construction of the continental slope and rise off southwestern Africa: *Marine Geology*, v. 37, p. 333-354, doi: 10.1016/0025-3227(80)90109-7.
- Dott, R.H., 1963, Dynamics of subaqueous gravity depositional processes: *AAPG Bulletin*, v. 47, p. 104-128.
- Dugan, B., 2012, Petrophysical and consolidation behavior of mass transport deposits from the northern Gulf of Mexico, IODP Expedition: *Marine Geology*, v. 315-318, p. 98-107, doi:10.1016/j.margeo.2012.05.001.
- Expedition 308 Scientists, 2005, Overpressure and fluid flow processes in the deepwater Gulf of Mexico: slope stability, seeps, and shallow-water flow. IODP Prel. Rept., 308, doi:10.2204/iodp.pr.308.2005.
- Fine, I.V., Rabinovich, A.B., Bornhold, B.D., Thomson, R.E., and Kulikov, E.A., 2005, The Grand Banks landslide-generated tsunami of November 18, 1929: preliminary analysis and numerical modeling: *Marine Geology*, v. 215, p. 45-57, doi:10.1016/j.margeo.2004.11.007.
- Frey-Martinez, J., Cartwright, J., and Hall, B., 2005, 3D seismic interpretation of slump complexes: Examples from the continental margin of Israel: *Basin Research*, v. 17, p. 83-108, doi: 10.1111 /j.1365-2117.2005.00255.x.
- Gee, M.J.R., Gawthorpe, R.L., and Friedmann, S.J., 2006, Triggering and evolution of a giant submarine landslide, offshore Angola, revealed by 3D seismic stratigraphy and geomorphology: *Journal of Sedimentary Research*, v. 76, p. 9-19, doi: 10.2110/jsr.2006.02.
- Georgiopoulou, A., Masson, D.G., Wynn, R.B., and Krastel, S., 2010, Sahara Slide: Age, initiation, and processes of a giant submarine slide: *Geochemistry, Geophysics, Geosystems*, v. 11, p. Q07014, doi: 10.1029/2010GC003066.
- Gong, Z.S., and Li, S.T., 1997, Continental Margin Basin Analysis and Hydrocarbon Accumulation of the Northern South China Sea. Science Press, Beijing, pp. 193-256.
- Haflidason, H., Lien, R., Sejrup, H.P., Forsberg, C.F., and Bryn, P., 2005, The dating and morphometry of the Storegga Slide: *Marine and Petroleum Geology*, v. 22, p. 123-136, doi: 10.1016/j.marpetgeo.2004.10.008.
- Haflidason, H., Sejrup, H.P., Nygard, A., Mienert, J., Bryn, P., Lien, R., Forsberg, C.F., Berg, K. and Masson, D., 2004, The Storegga Slide: architecture, geometry and slide development: *Marine Geology*, v. 213, p. 201-234,

10.1016/j.margeo.2004.10.007.

Hjelstuen, B.O., Eldholm, O., and Faleide, J.I., 2007, Recurrent Pleistocene mega-failures on the SW Barents Sea margin: *Earth and Planetary Science Letters*, v. 258, p. 605-618, doi: 10.1016/j.epsl.2007.04.025.

Lamarche, G., Joanne, C., and Collot, J.Y., 2008, Successive, large mass-transport deposits in the south Kermadec fore-arc basin, New Zealand: The Matakaoa Submarine Instability Complex: *Geochemistry Geophysics Geosystems*, v. 9, Q04001, doi: 10.1029/2007GC001843.

Lee, C., Nott, J.A., and Keller, F.B., 2004, Seismic expression of the Cenozoic mass transport complexes, deepwater Tarfaya-Agadir basin, offshore Morocco: Houston, Texas, Offshore Technology Conference Proceedings, OTC16741.

Leslie, S.C., and Mann, P., 2016, Giant submarine landslides on the Colombian margin and tsunami risk in the Caribbean Sea: *Earth and Planetary Science Letters*, v. 449, p. 382-394, doi: 10.1016/j.epsl.2016.05.040.

Locat, J., Lee, H.J., Locat, P., and Imran, J., 2004, Numerical analysis of the mobility of the Palos Verdes Debris avalanche, California, and its implications for the generation of tsunamis: *Marine Geology*, v. 203, p. 269–280, [https://doi.org/10.1016/S0025-3227\(03\)00310-4](https://doi.org/10.1016/S0025-3227(03)00310-4).

Maslin, M.A., Owen, M.J., Day, S., and Long, D., 2004, Linking continental-slope failures and climate change: Testing the clathrate gun hypothesis: *Geology*, v. 32, p. 53-56, doi: 10.1130/G20114.1.

Masson, D.G., Watts, A.B., Gee, M.J.R., Urgeles, R., Mitchell, N.C., Le Bas, T.P., and Canals, M., 2002, Slope failures on the flanks of the western Canary Islands: *Earth-Science Reviews*, v. 57, p. 1-35, [https://doi.org/10.1016/S0012-8252\(01\)00069-1](https://doi.org/10.1016/S0012-8252(01)00069-1).

Moscardelli, L., and Wood, L., 2008, New classification system for mass transport complexes in offshore Trinidad: *Basin Research*, v. 20, p. 73-98, doi: 10.1111/j.1365-2117.2007.00340.x.

Moscardelli, L., and Wood, L., 2015, Morphometry of mass-transport deposits as a predictive tool: *GSA Bulletin*, v. 128, p. 47-80, doi: 10.1130/B31221.1.

Mosher, D.C., Shimeld, J., Hutchinson, D., Lebedeva-Ivanova, N., and Chapman, C.B., 2012, Submarine landslides in Arctic sedimentation: Canada basin, in Yamada, Y., Kawamura, K., Ikehara, K., Ogawa, Y., Urgeles, R., Mosher, D., Chaytor, J., and Strasser, M., eds., *Submarine Mass Movements and Their Consequences: Dordrecht, Springer, Advances in Natural and Technological Hazards Research*, v. 31, p. 147-157.

Nardin, T.R., Hein, F.J., Gorsline, D.S., and Edwards, B.D., 1979, A review of mass movement processes, sediment, and acoustic characteristics and contrasts in slope and base-of-slope systems versus canyon-fan-basin floor systems: *SEPM Special Publication*, v. 27, p. 61-73.

Niemi, T.M., Ben-Avraham, Z., Hartnady, C.J.H., and Reznikov, M., 2000, Post-Eocene seismic stratigraphy of the deep

- ocean basin adjacent to the southeast African continental margin: A record of geostrophic bottom current systems: *Marine Geology*, v. 162, p. 237-258, doi: 10.1016/S0025-3227(99)00062-6.
- Ogiesoba, O., and Hammes, U., 2012, Seismic interpretation of mass-transport deposits within the upper Oligocene Frio Formation, south Texas Gulf Coast: *AAPG Bulletin*, v. 96, p. 845-868, doi:10.1306/09191110205.
- Owen, M., Day, S., and Maslin, M., 2007, Late Pleistocene submarine mass movements: occurrence and causes: *Quaternary Sciences Reviews*, v. 26, p. 958-978, doi:10.1016/j.quascirev.2006.12.011.
- Owen, M., Day, S., Long, D., and Maslin, M., 2010, Investigations on the Peach 4 Debrite, a Late Pleistocene mass movement on the northwest British continental margin, in Mosher, D.C., Shipp, R.C., Moscardelli, L., Chaytor, J.D., Baxter, C.D.P., Lee, H.J., and Urgeles, R., eds., *Submarine Mass Movements and Their Consequences: Dordrecht, Springer, Advances in Natural and Technological Hazards Research*, v. 28, p. 301-311.
- Piper, D.J.W., Pirmez, C., Manley, P.L., Long, D., Food, R.D., Normark, W.R., and Showers, W., 1997, Mass-transport Deposits of the Amazon Fan, in R.D. Flood, D.J.W. Piper, A. Klaus, and L.C. Peterson (eds.), *Proceedings of the Ocean Drilling Program, Scientific Results*, v. 155, p. 109-146.
- Pope, E.L., Talling, P.J., and Carter, L., 2017, Which earthquakes trigger damaging submarine mass movements: Insights from a global record of submarine cable breaks?: *Marine Geology*, v. 384, p. 131-146, doi: 10.1016/j.margeo.2016.01.009.
- Popenoe, P., Schmuck, E.A., and Dillon, W.P., 1993, The Cape Fear Landslide: slope failure associated with salt diapirism and gas hydrate decomposition. In: *Submarine landslides: selective studies in the U.S. Exclusive Economic Zone*. U.S. Geological Survey Bulletin, v. 2002, p. 40-53.
- Shipboard Scientific Party, 1995. Site 941. In Flood, R.D., Piper, D.J.W., Klaus, A., et al., *Proc. ODP, Init. Repts.*, 155: College Station, TX (Ocean Drilling Program), 503-536, doi:10.2973/odp.proc.ir.155.117.1995.
- Shipp, R.C., Nott, J.A., and Newlin, J.A., 2004, Physical Characteristics and Impact of Mass Transport Complexes on Deepwater Jetted Conductors and Suction Anchor Piles (In: *Offshore Technology Conference, Houston, Texas*), OTC16751.
- Strasser, M., Moore, G.F., Kimura, G., Kopf, A.J., Underwood, M.B., Guo, J.H., and Sreaton, E.J., 2011, Slumping and mass transport deposition in the Nankai fore arc: evidence from IODP drilling and 3-D reflection seismic data: *Geochemistry Geophysics Geosystems*, v. 12, Q0AD13, doi:10.1029/2010GC003431.
- Sun, Q.L., Alves, T., Xie, X.N., He, J.X., Li, W., and Ni, X.L., 2017b, Free gas accumulations in basal shear zones of mass-transport deposits (Pearl River Mouth Basin, South China Sea): An important geohazard on continental slope basins: *Marine and Petroleum Geology*, v. 81, p. 17-32, <http://dx.doi.org/10.1016/j.marpetgeo.2016.12.029>.
- Sun, Q.L., Xie, X.N., Piper, D.J.W., Wu, J., and Wu, S.G., 2017a, Three dimensional seismic anatomy of multi-stage mass

- transport deposits in the Pearl River Mouth Basin, northern South China Sea: Their ages and kinematics: *Marine Geology*, v. 393, p. 93-108, doi: 10.1016/j.margeo.2017.05.005.
- Synolakis, C.E., Bardet, J.P., Borrero, J., Davies, H.L., Okal, E.A., Silver, E.A., Sweet, S., and Tappin, D.R., 2002, The slump origin of the 1998 Papua New Guinea Tsunami: *Proceedings: Mathematical, Physical and Engineering Sciences*, v. 458, p. 763-789, doi: 10.1098/rspa.2001.0915.
- ten Brink, U.S., Geist, E.L., and Andrews, B.D., 2006, Size distribution of submarine landslides and its implication to tsunami hazard in Puerto Rico: *Geophysical Research Letters*, v. 33, p. L11307, doi: 10.1029/2006GL026125.
- Torelli, L., Sartori, R., and Zitellini, N., 1997, The giant chaotic body in the Atlantic Ocean off Gibraltar: New results from a deep seismic reflection survey: *Marine and Petroleum Geology*, v. 14, p. 125-138, doi: 10.1016/S0264-8172(96)00060-8.
- Trincardi, F., and Argnani, A., 1990, Gela submarine slide: A major basin-wide event in the Plio-Quaternary fore deep of Sicily: *Geo-Marine Letters*, v. 10, p. 13-21, doi: 10.1007/BF02431017.
- Tripsanas, E.K., Piper, D.J.W., Jenner, K.A., and Bryant, W.R., 2008, Submarine mass-transport facies: new perspectives on flow processes from cores on the eastern North American margin: *Sedimentology*, v. 55, p. 97-136, doi: 10.1111/j.1365-3091.2007.00894.x.
- Vanneste, M., Mienert, J., and Bünz, S., 2006, The Hinlopen Slide: A giant, submarine slope failure on the northern Svalbard margin, Arctic Ocean: *Earth and Planetary Science Letters*, v. 245, p. 373-388, doi: 10.1016/j.epsl.2006.02.045.
- Völker, D.J., 2010, A simple and efficient GIS tool for volume calculations of submarine landslides: *Geo-marine Letters*, v. 30, p. 541-547, doi: 10.1007/s00367-009-0176-0.
- Wang, P.X., Prell, W., Blum, P., and the Leg 184 Scientific Party, 1999, Exploring the Asian Monsoon through Drilling in the South China Sea: *JOIDES Journal*, v. 25, p. 8-13.
- Wessel, P., and Smith, W.H.F., 1998, New, improved version of Generic Mapping Tools released, *EOS, Transactions, American Geophysical Union*, v. 79, p. 579.
- Wynn, R.B., Masson, D.G., Stow, D.A.V., and Weaver, P.P.E., 2000, The Northwest African slope apron: A modern analogue for deep-water systems with complex seafloor topography: *Marine and Petroleum Geology*, v. 17, p. 253-265, doi: 10.1016/S0264-8172(99)00014-8.
- Xie, H., Zhou, D., Li, Y.P., Pang, X., Li, P.C., Chen, G.H., Li, F.C., and Cao, J.H., 2014, Cenozoic tectonic subsidence in deepwater sags in the Pearl River Mouth Basin, northern South China Sea: *Tectonophysics*, v. 615-616, p. 182-198, doi: 10.1016/j.tecto.2014.01.010.
- Zhu, W., Huang, B., Mi, L., Wilkins, R.W., Fu, N., and Xiao, X., 2009, Geochemistry, origin, and deep-water exploration

potential of natural gases in the Pearl River Mouth and Qiongdongnan Basins, South China Sea: AAPG Bulletin, v. 93,  
p. 741-761, doi:10.1306/02170908099.

Accepted Article

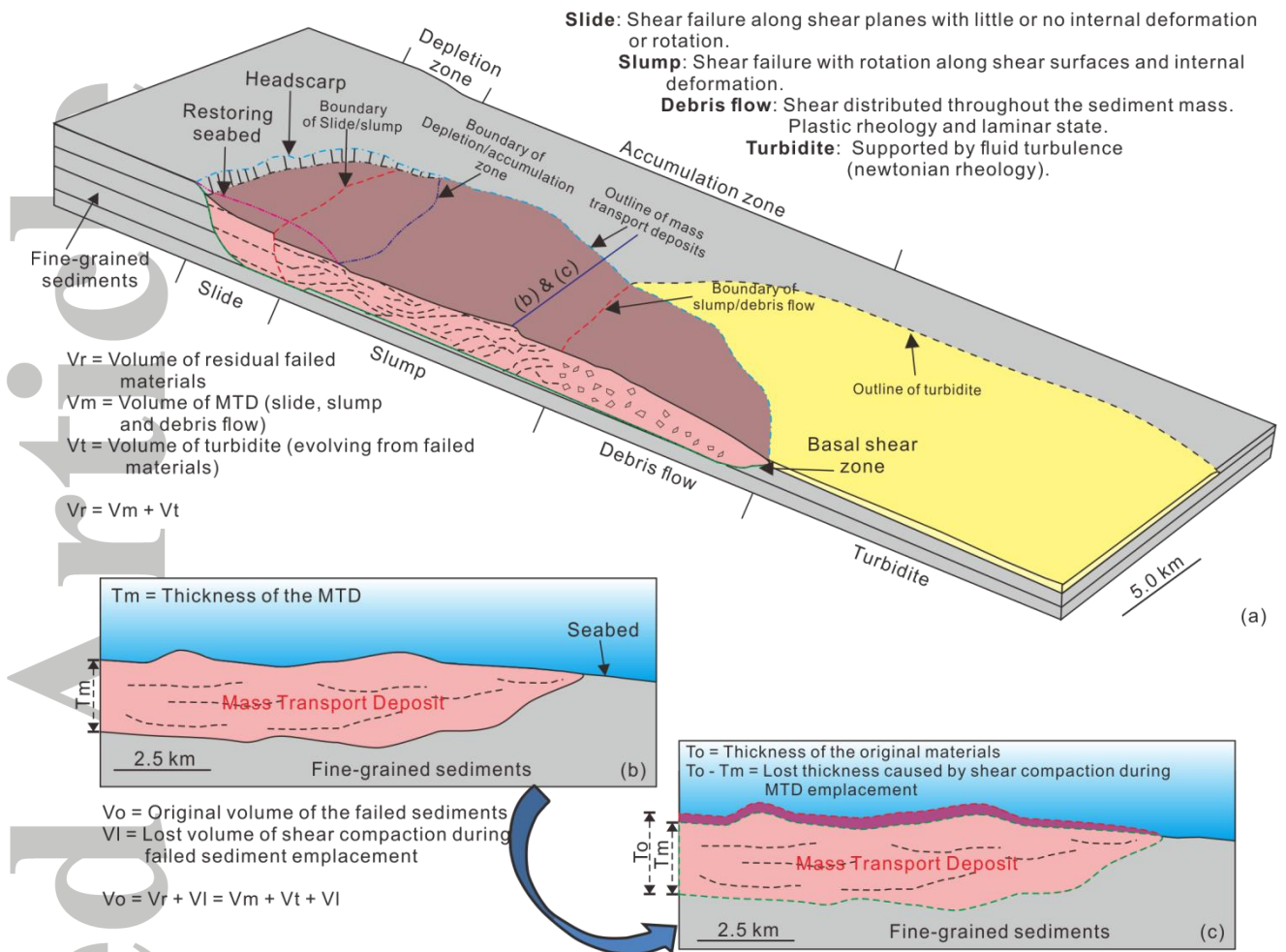


Figure 1: Schematic representation of a submarine landslide and corresponding volume estimates. (a) Failed sediments are composed of MTDs (slides, slumps and debris flows) and turbidites. The residual volume of failed sediments ( $V_r$ ) includes the volumes of imaged MTDs ( $V_m$ ) and sub-seismic turbidities ( $V_t$ ); (b) and (c) shear compaction during the transport and emplacement of the failed sediment results in volume losses. As a result, the present-day thickness ( $T_m$ ) of MTDs is less than their original thickness ( $T_o$ ), which precluded the effect of shear compaction on the displaced sediment. The original volume representing the volume before the occurrence of slope failure comprises the volume of the mapped MTDs ( $V_m$ ), sub-seismic turbidities ( $V_t$ ) and losses in volume due to shear compaction ( $V_I$ ).

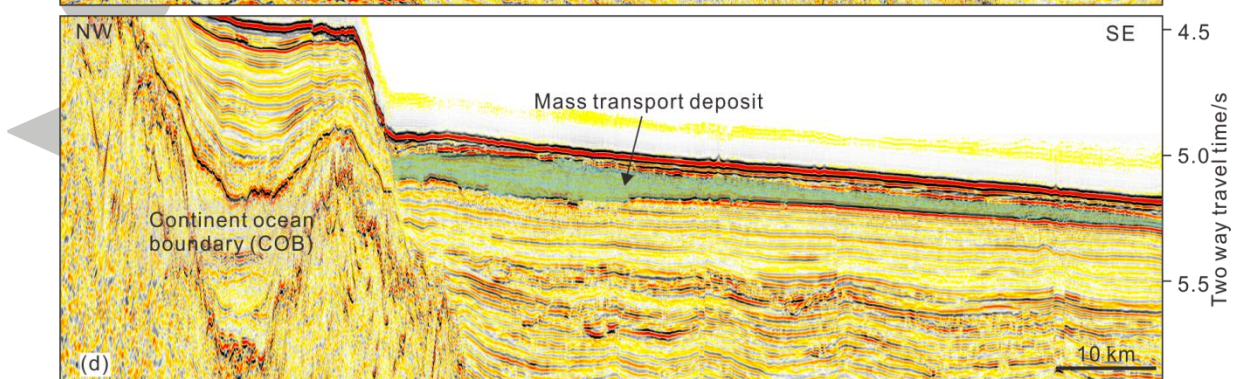
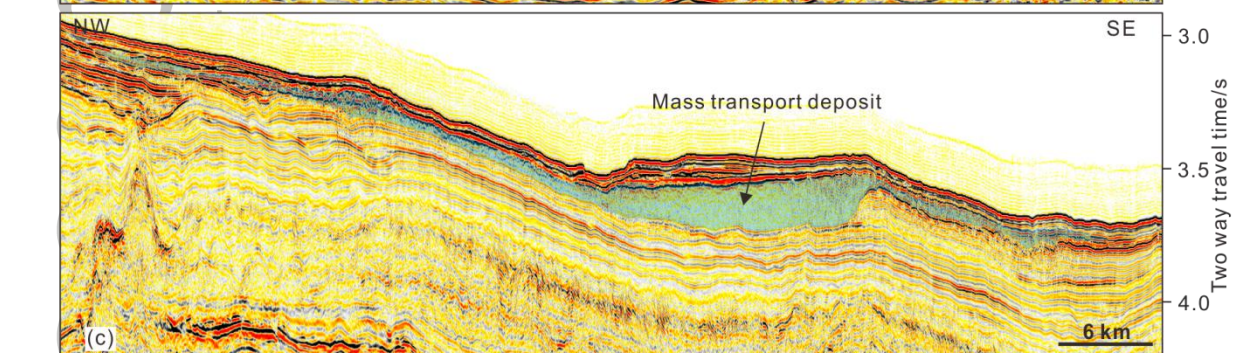
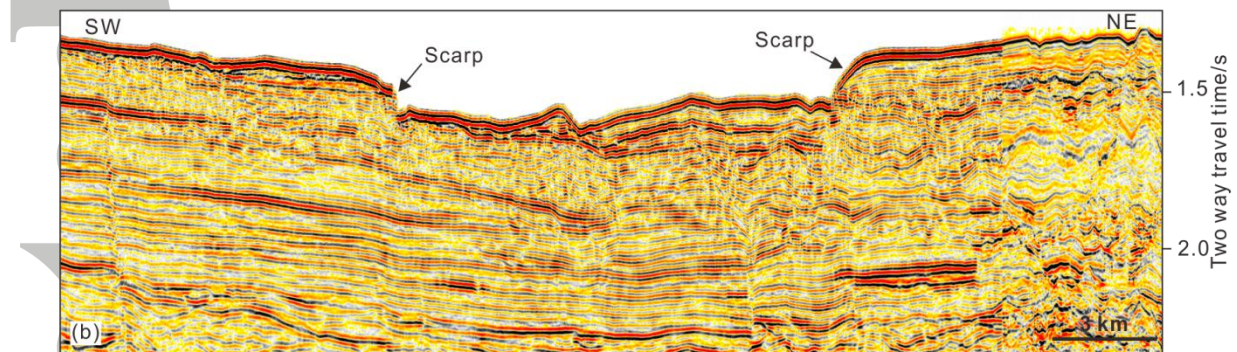
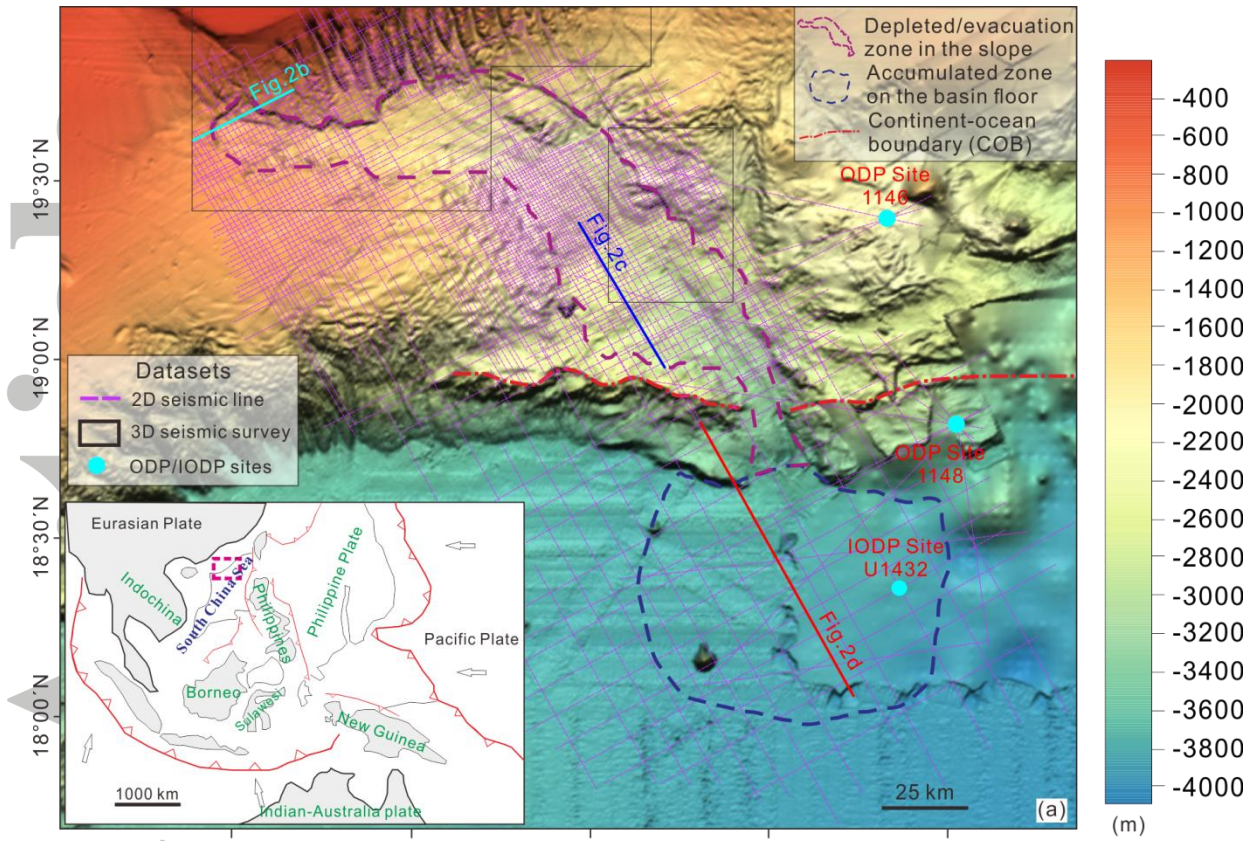


Figure 2: Multibeam bathymetric and reflection seismic characteristics of slope failures in the northern South China Sea. (a) Large scarps characterize the continental slope area (purple dashed line), which is connected to the fan-shaped ocean basin (dark-blue dashed line) by a wide moat at the Continent-Ocean Boundary (COB). The datasets of 2D/3D seismic surveys are labeled. Left-bottom corner: regional background of the study area; (b) 2-D seismic profile crossing the headwall zone (upper slope) of the slope failure, in which extensional structures are not observed; (c) 2-D seismic profile crossing the lower slope highlighting the chaotic interpreted character of the studied MTD; (d) 2-D seismic profile crossing the ocean basin and showing an MTD scattered away from the interpreted moat.

Accepted Article

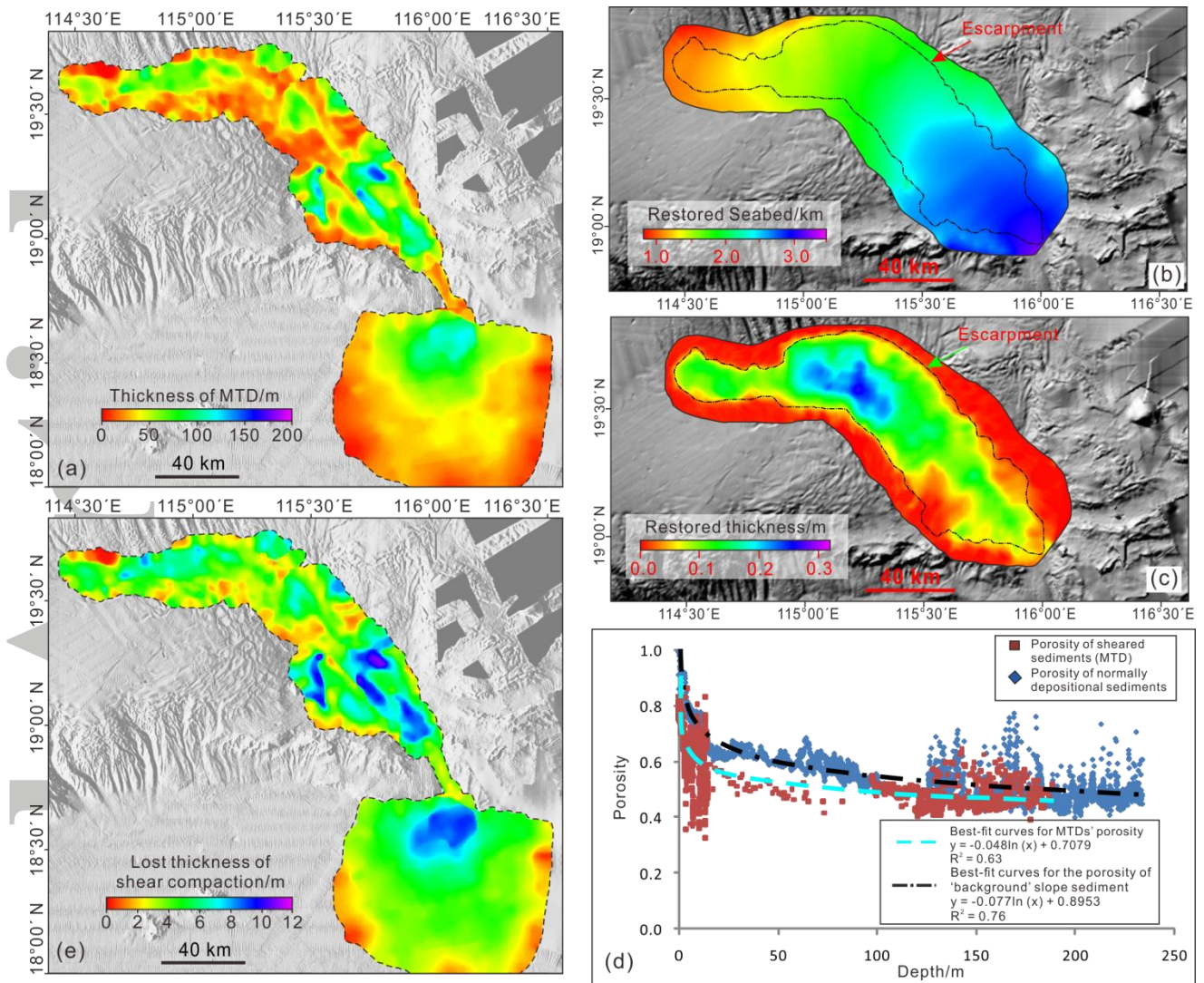


Figure 3: Volume calculation of slope failure in the study area. (a) MTD thickness as imaged by detailed seismic maps; (b) Restored seabed morphology after healing the escarpment; (c) Restored thickness between the present-day and the restored pre-failure sea bed; (d) Best-fit curves for fine-grained 'background' slope sediment and MTDs; (e) Thickness losses caused by shear and normal compaction.

Accept